Magnetoelastic coupling in RETiO$_3$ (RE = La, Nd, Sm, Gd, Y)

A. C. Komarek,[1] H. Roth,[1] M. Cwik,[1] W.-D. Stein,[1] J. Baier,[1] M. Kriener,[1] F. Bourée,[2] T. Lorenz,[1] and M. Braden[1,*]

[1] *II. Physikalisches Institut, Universität zu Köln, Zülpicher Str. 77, D-50937 Köln, Germany*
[2] *Laboratoire Léon Brillouin, CEA-CNRS, CE-Saclay, F-91191 Gif-sur-Yvette, France*

(Dated: February 6, 2008)

A detailed analysis of the crystal structure in RETiO$_3$ with RE = La, Nd, Sm, Gd, and Y reveals an intrinsic coupling between orbital degrees of freedom and the lattice which cannot be fully attributed to the structural deformation arising from bond-length mismatch. The TiO$_6$ octahedra in this series are all irregular with the shape of the distortion depending on the RE ionic radius. These octahedron distortions vary more strongly with temperature than the tilt and rotation angles. Around the Ti magnetic ordering all compounds exhibit strong anomalies in the thermal-expansion coefficients, these anomalies exhibit opposite signs for the antiferromagnetic and ferromagnetic compounds. Furthermore the strongest effects are observed in the materials close to the magnetic cross-over from antiferromagnetic to ferromagnetic order.

I. INTRODUCTION

The rare-earth titanates (RETiO$_3$) with a distorted perovskite structure have a single electron in the t_{2g} orbitals of the Ti-3d shell and are all Mott insulators[1]. Therefore, they can be considered as the one-electron counterpart to the cuprates with a single hole in the 3d shell. Upon decreasing the ionic radius in the rare-earth RE series from La to Y[2], the calculated one-electron bandwidth gets smaller[3] and the deviation of the Ti-O-Ti bond angle from 180° increases[4]. Concomitantly, the Ti magnetic order changes from G-type antiferromagnetism with the magnetic moment in a direction (RE = La,...,Sm) to ferromagnetism with the magnetic moment in c direction (RE=Gd,...,Yb and Y)[5,6,7,8,9,10,11,12,13,14,15,16] . These apparently distinct magnetic ordering schemes, however, belong to the same irreducible representation, as it has been clarified long ago[17] for the structure type of GdFeO$_3$ to which all RETiO$_3$ belong. Due to the low symmetry of the crystal structure, the G-type antiferromagnetic component in a direction is always coupled with an A-type antiferromagnetic moment in b direction and a ferromagnetic component in c direction. Thus the change from antiferromagnetic to ferromagnetic order of the Ti moments in the series of RETiO$_3$ is just a redistribution of the ordered moment between the three different components (G_x, A_y and F_z) within the same magnetic symmetry.

Tremendous efforts have been made to understand the magnetic properties of these titanates during the last years[18,19,20,21,22,23,24,25]. An orbital liquid model has been proposed in the idea that the splitting between the t_{2g} states would be sufficiently low to allow orbital fluctuations to play a dominant role in the physical properties[20,21]. On the other hand, in a more conventional scenario, it is argued that orbital fluctuations would be efficiently suppressed by the t_{2g}-level splitting of the order of 200 meV[5,22,23,26,27]. Taking account of the anisotropic orbital arrangement Schmitz and Müller-Hartmann could explain nearly all the details of the magnetic order in LaTiO$_3$ including the measured dispersion of the magnetic excitations[24,25].

In addition to the Ti magnetism, magnetic order of the RE moments occurs at lower temperature. For the lighter RE ions (RE = Ce, ... , Sm) the RE moments order antiferromagnetically below $T_{N2} < T_{N1}$ (with T_{N1} being the Néel temperature for G_x-type antiferromagnetic ordering at the Ti sites). For the RETiO$_3$ compounds studied in this work belonging to this first group (RE = Nd, Sm) an antiferromagnetic ordering of F_y/C_z-type is observed at the RE sites[6,7]. For the RETiO$_3$ with heavier RE ions (RE = Gd,...,Yb) there are two basic magnetic structures. In the first class, the RE magnetic moments order ferromagnetically and couple antiparallel to the ferromagnetic component of the Ti sites (F_z). In the second class (RE=Tb, Dy and Ho) the magnetic moments at the RE sites have both ferromagnetic and antiferromagnetic components in the a, b plane[16,28,29,30,31]. Among the heavier RETiO$_3$ materials only GdTiO$_3$ has been studied in this work, it exhibits ferromagnetic Gd-moment ordering (first group). These complex RE magnetic structures, however, seem to yield little insight to the Ti magnetism and the associated interaction energies are smaller than those in-between the Ti's except in the compounds where the Ti-Ti interaction is strongly suppressed.

The GdFeO$_3$-type structure of the rare-earth titanates differs from the ideal, cubic perovskite structure (with space group $Pm\overline{3}m$) by a rotation of the octahedra around the c axis and by an additional tilt of the TiO$_6$ octahedra around the cubic [110] axis. While the octahedral tilts are opposite for all neighboring TiO$_6$ octahedra, the octahedra are rotated in the same sense along the c direction and opposite only in the ab planes. The combination of tilt and rotation distortion reduces the symmetry to the orthorhombic space group $Pbnm$ and enlarges the unit cell to a $\sqrt{2} \times \sqrt{2} \times 2$ cell rotated by 45° around the c axis (see Fig 1). In this space group internal distortions of the TiO$_6$ octahedra can occur without a further symmetry breaking. The most famous example for such additional distortions is LaMnO$_3$ where the antiferroorbital order of the e_g electrons coexists with the tilt and the rotation[32,33,34]. Qualita-

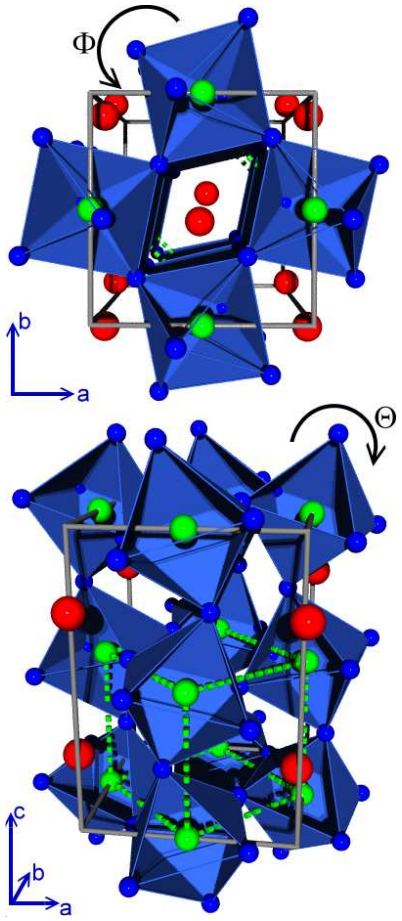

FIG. 1: (color online) Crystal structure of RETiO$_3$ with corner sharing TiO$_6$ octahedra in *Pbnm* notation. Dashed lines show the cubic unit cell of the undistorted structure and solid lines show the orthorhombic unit cell. *Green:* Ti-ions, *blue:* O-ions and *red:* *RE*-ions.

tively similar octahedron distortions have been observed for all rare earth titanates studied in this work[4,5]. For an undistorted octahedron, one expects a negative orthorhombic splitting $\varepsilon = (a-b)/(a+b)$ since the octahedral tilt takes place around the orthorhombic b axis (*Pbnm*). But due to an elongation of the TiO$_6$ octahedraon basal plane along the orthorhombic a direction the orthorhombic splitting in LaTiO$_3$ becomes even positive. In the series of RETiO$_3$ the type of octahedral distortion changes its character with decreasing rare-earth ionic radius. For LaTiO$_3$ the O2-O2 distances (O1 denotes the apical oxygen displaced from the Ti sites along c and O2 the basal in-plane oxygen) along the octahedron edges differ strongest resulting in a rectangular shape of the basal oxygen planes. In contrast, in YTiO$_3$ there is little difference in these O2-O2 distances but the two in-plane Ti-O2 distances split. These distortions together with the anisotropic Ti-*RE* coordination lead to a splitting of the t_{2g} energy levels with a different character of the lowest state. Interestingly the orbital arrangement resulting from these two distortions is totally different. Within a single layer parallel to the a, b plane, the variation of the edge lengths yields a ferroorbital configuration whereas the splitting of the Ti-O2 distances yields an antiferroorbital configuration[5]. According to Goodenough-Kanamori rules, these distinct orbital ordering schemes agree with the antiferromagnetic and ferromagnetic Ti ordering in LaTiO$_3$ and in YTiO$_3$, respectively.

Although there is no doubt that the octahedron distortions in the RETiO$_3$ series are coupled with the magnetic ground state, it is less obvious whether these effects should be considered as resulting from orbital ordering. There is no symmetry breaking in the titanate case as the orbital distortions are embedded in the crystal structure deformation arising from tilt and rotation. Pavarini et al.[23] argue that the values of the tilting and the concomitant shift of the *RE* sites would determine the splitting of the orbital levels[23]. However, the lattice parameters and the octahedron deformation in LaTiO$_3$ exhibit clear anomalies around the magnetic ordering suggesting that there is an intrinsic coupling between orbital degrees of freedom and the crystal structure[5,35]. It is the aim of the present work to further elucidate this orbital-lattice coupling in the RETiO$_3$ series and to separate the intrinsically electronic effects from tilt and rotation distortions. For this purpose we have analyzed the known crystal structure of oxides showing the same GdFeO$_3$ structure type but having no electron in the 3*d* shell. Furthermore we have studied the temperature dependence of the crystal structure in RETiO$_3$ for RE = La, Sm, Nd, Gd, and Y in great detail. In all compounds we find evidence for a direct orbital-lattice coupling in addition to that arising from the distortions.

II. EXPERIMENTAL

Single crystals of RETiO$_3$ were grown using a floating-zone image furnace, as described elsewhere[36]. Parts of them were crushed in order to obtain powder samples of high quality. Magnetic ordering temperatures of the Ti ions were determined by a SQUID or a vibrating sample magnetometer. The magnetic ordering of the Ti depends sensitively on the stoichiometry RE_{1-x}TiO$_{3+\delta}$. In order to obtain crystals with a high transition temperature it is necessary to tune the parameters during the growth process. In this work several crystals of the same material were grown and analysed; the highest T_N/T_C-values, we find, agree with or are higher than those reported in a recent study[16]. The Néel temperatures of the antiferromagnetic compounds are 146 K for LaTiO$_3$; 94 K and 81 K for two samples of NdTiO$_3$ and 54 K and 48 K for two crystals of SmTiO$_3$. In the case of NdTiO$_3$ the high T_N-sample was used for diffraction and thermal expansion studies and the lower T_N-sample only for diffraction studies. For SmTiO$_3$, the 54 K sample was studied in thermal expansion and the 48 K sample by diffraction techniques. The Curie temperatures for the

ferromagnetic titanates are 36 K (RE=Gd) and 29 K and 25 K for two $YTiO_3$ samples used for diffraction and thermal expansion measurements, respectively. The Several diffraction techniques were applied to analyze the temperature dependencies of the structural parameters. A Siemens D5000 diffractometer equipped with a one-dimensional detector was used for powder X-ray diffraction with Cu-K_α or Cr-K_α radiation. These as well as the neutron powder diffraction data were analyzed by the Rietveld technique, but the laboratory X-ray powder diffraction does not allow one to obtain the oxygen structural parameters. In order to perform full structure analyzes powder neutron-diffraction patterns were recorded on the high-resolution 3T.2 diffractometer at the Orphée reactor in Saclay (λ = 1.2251Å). The full crystal structure is also determined by single-crystal X-ray diffraction studies on a *Bruker X8 Apex* CCD diffractometer using Mo-K_α radiation. Absorbtion correction for spherical samples was performed with the standard *Bruker* software (*scale*) and isotropic extinction correction was applied during the refinement on F^2 with *Jana*2000[38]. Some of the crystals were twinned. Due to very similar lattice parameter in $LaTiO_3$, the components of all twin domains could be integrated together and refined with different volume fractions for all twin domains within *Jana*2000. The corresponding twin laws result from a threefold rotation about the [111] axis of the 8 Å pseudocube combined with a reflection across the (1-10) plane. In the other $RETiO_3$, no twinning was observable or the contributions of the different twins could be separated during integration procedure thus obtaining a dataset only for the major twin domain. This was the case in $NdTiO_3$, where the reflections of different twin domains which could not be separated from each other were dismissed (see also Tab. I). These minor twin domains have only small volume fractions of roughly 10% of the total sample volume. The structural results of our single crystal X-ray and powder neutron-diffraction experiments are summarized in Tab. I & II. Thermal-expansion coefficients were measured for single-crystalline $YTiO_3$, $SmTiO_3$, and $NdTiO_3$ on a high-resolution capacitance dilatometer[39]. For $YTiO_3$ we furthermore measured the magnetostriction along the a direction in magnetic fields up to 14 T.

III. RESULTS AND DISCUSSION

A. Analysis of known $GdFeO_3$-type structures

Since it is not obvious in the $RETiO_3$ series to separate the intrinsic orbital-ordering effects from those imposed by the severe tilt and rotation distortions, it appeared interesting to analyze the published crystal structures of metal oxides AMO_3 in $GdFeO_3$-type structure which posses an empty $3d$ shell. Using the Inorganic Crystal Structure Database (ICSD)[40] we have studied the compounds : $CaTiO_3$, $CaZrO_3$, $EuScO_3$, $GdGaO_3$, $GdScO_3$,

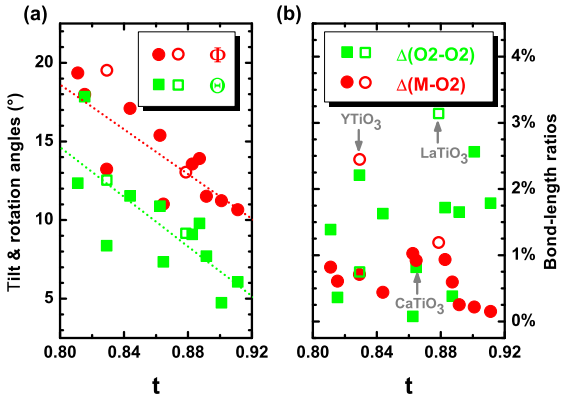

FIG. 2: (color online) (a) The octahedral tilt Θ and the rotation Φ versus the tolerance factor t for various d^0 systems with perovskite structure (space group number 62, Pbnm[37]). (b) Difference of both basal M-O2 bond lengths and difference of both O2-O2 bond lengths versus t. (Open symbols denote the values for $LaTiO_3$ and $YTiO_3$; lines are linear fits to the data.)

$HoAlO_3$, $LaGaO_3$, $NdGaO_3$, $PrGaO_3$, $SmAlO_3$, $SrZrO_3$, $TbAlO_3$ with respect to their tilting (Θ) and rotation (Φ) distortions and to the deformation of the metal-oxygen octahedron.[41] We discuss the relative difference between the two M-O2 distances, $\Delta(M-O2)$, and that between the two O2-O2 basal-plane edge lengths, $\Delta(O2-O2)$. The analysis of the published structures is resumed in Fig. 2. The tilt and rotation deformations arise from the bond-length mismatch between the M-O and A-O bonds which in the case of an ideal perovskite would be forced into a ratio of $\sqrt{2}$. With the ionic radii[2] one calculates the tolerance factor $t = (r_A + r_O)/[\sqrt{2}\cdot(r_M + r_O)]$ with values much below $t = 1$ indicating a strong mismatch due to too small A ionic radii. Fig. 2 (a) shows the tilt and rotation angles as a function of the tolerance factor yielding the expected increase of both distortions towards smaller tolerance factors. Also the ratio between the tilt and rotation angles seems to be fully determined by the tolerance factor. One may note that $LaTiO_3$ and $YTiO_3$ match these relations. In Fig. 2 (b) we show the $\Delta(M-O2)$ and $\Delta(O2-O2)$ values again as a function of the tolerance factor. For the $\Delta(M-O2)$ bond-distance ratio there is no clear tolerance-factor dependence visible, but the deformation of about 2.5% seen in $YTiO_3$ is much larger than those in all the others materials which vary only between 0% and 1%. This gives the first evidence that the $\Delta(M-O2)$ deformation is not purely a consequence of the tilt and the rotation in the titanates. Concerning the edge-length deformation characterized by $\Delta(O2-O2)$, the deformation of about 3% seen in $LaTiO_3$ is strongest but there seems to be a sizeable distortion also in the series without $3d$ electrons. This deformation is intimately coupled with the orthorhombic splitting. Tilting of a rigid octahedron around b will always yield a smaller a lattice parameter, whereas some of the

materials, including $LaTiO_3$, show the opposite. This reversed orthorhombic splitting, however, appears only for small tilt angles. It seems to result from the interactions between the A site and the apical oxygens. One of these bond distances is significantly shortened by a rigid tilt. The systems may therefore elongate perpendicular to the tilt axis in order to reduce this effect. This will yield a weak elongation of the octahedron basal plane along a and eventually the reversed orthorhombic splitting. Although $LaTiO_3$ exhibits the strongest $\Delta(O2-O2)$ deviation, additional information is needed in order to clarify an underlying orbital effect.

B. Temperature dependence of the crystal structure in antiferromagnetic RETiO$_3$ (RE = La, Nd, Sm)

For the RE titanates with larger rare-earth ionic radius showing antiferromagnetic order, we observe a strong rise of the a lattice parameter at the onset of the magnetic ordering on cooling. Concomitantly, the b lattice parameter decreases more rapidly leading to a strong increase in the orthorhombic splitting $\varepsilon = (a-b)/(a+b)$ upon cooling. This anomalous behaviour of the a lattice parameter was first observed for $LaTiO_3$[5,35]. Our measurements on other RETiO$_3$ show that this anomalous rise of ε becomes even enhanced for smaller RE in the series of RETiO$_3$ as long as the system stays antiferromagnetic, see Fig. 3(e).

In Fig. 4 the results of powder neutron diffraction measurements on $LaTiO_3$ up to T=750 K are shown. The structure data at the first three temperatures were taken from Ref.[5] where the same sample as in the present study was used. Over the full temperature range, the variation of both the octahedral tilt Θ and the rotation Φ is very small, but the ratio of the O2-O2 octahedron edge lengths changes essentially, from approximately 4% at 10 K to approximately half of this value at 750 K. Thus only the internal octahedral distortions vary strongly with temperature. The decoupling of tilt and rotation angles on the one side and of the octahedron distortion on the other side demonstrates that the latter is not just a consequence of the former. The structural bond-length mismatch does not drive the octahedral distortion. Instead, the structural anomaly has to be ascribed to an orbital effect which, however, does not break any symmetry but just enhances the crystal-field splitting promoted through the tilt and rotation distortions.

Since the octahedral tilt Θ is nearly temperature independent, the rise of the orthorhombic splitting ε can be taken as an indicator for the elongation of the TiO_6 basal plane $\Delta(O2-O2)$, because only Θ and this distortion define the value of ε. Indeed, the plot of $\Delta(O2-O2)$ versus ε shows a linear dependence (see Fig. 4).

As can be seen in Fig. 3, the low-temperature increase of ε is more pronounced for the RETiO$_3$ with smaller RE, $NdTiO_3$ and $SmTiO_3$, still showing antiferromagnetic order. Furthermore, with decreasing rare-earth ionic radius the rise of ε starts closer to the magnetic ordering temperature, even though it sets in well above T_N for all samples studied. In $SmTiO_3$ with a T_N of only 45 K the anomalies are most pronounced. The increase of ε by 0.01 between 100 K and 10 K indicates an enhancement of the octahedral distortion characterized by $\Delta(O2-O2)$ by 1% , which is quite remarkable for an internal structure parameter. For $SmTiO_3$ the temperature dependence of the crystal structure has been studied by single-crystal X-ray diffraction down to 100 K. Again there is almost no variation in the rotation and tilt angles whereas the internal octahedral deformation significantly changes. Compared to $LaTiO_3$ the increase of $\Delta(O2-O2)$ between 300 and 100 K is much smaller but most likely much stronger between 100 K and lowest tem-

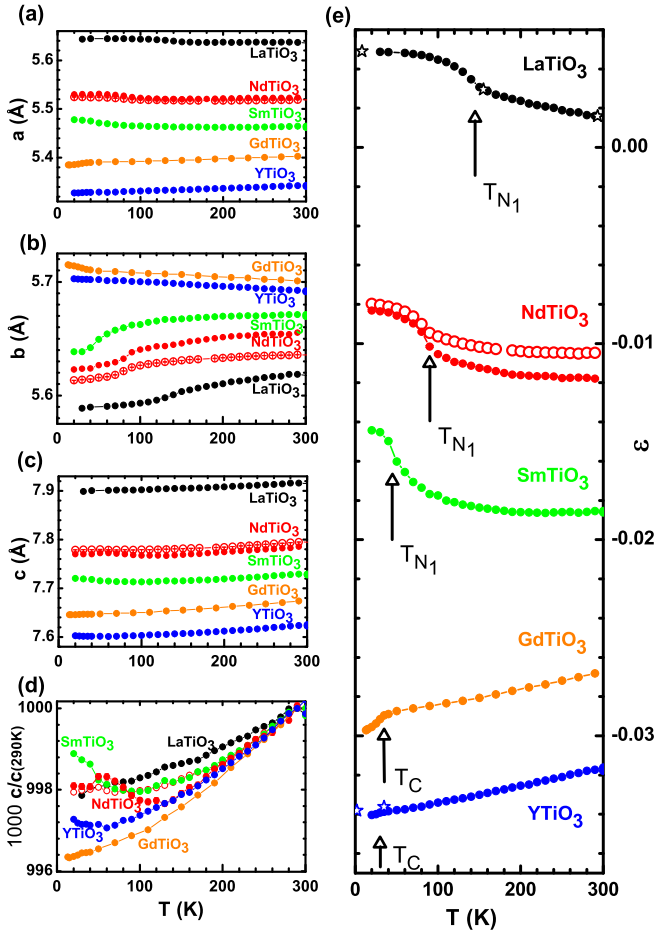

FIG. 3: (color online) (a-c) Orthorhombic lattice parameters of RETiO$_3$ (RE=La, Nd, Sm, Gd and Y) as a function of temperature. (d) c parameter scaled to the room temperature value. (e) Orthorhombic splitting $\varepsilon = (a-b)/(a+b)$. The arrows indicate the magnetic transition temperatures T_{N1} / T_C and the stars mark the values for ε measured by powder neutron diffraction. Open circles denote the values for the second $Nd_{1-x}TiO_{3+\delta}$ sample with a different stoichiometry and T_N = 81 K.

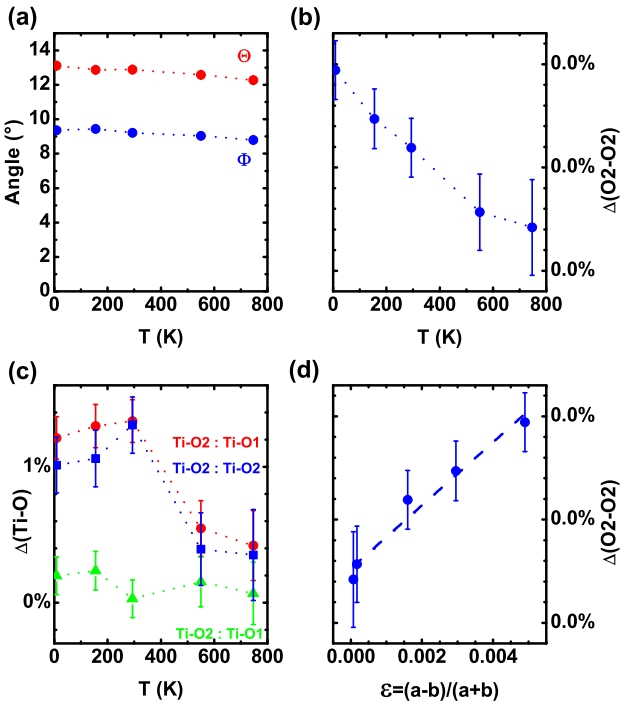

FIG. 4: (color online) Results of our powder neutron diffraction measurements on $LaTiO_3$ at different temperatures. The first three points were taken from Ref.[5]. The others were measured on the same sample. (a) TiO_6 octahedral tilt Θ and rotation Φ. (b) Differences of the O2-O2 bond lengths. (c) Differences of the Ti-O bond lengths. (d) Differences of the O2-O2 bond lengths versus ε. The approximately linear dependence of Δ(O2-O2 bond length) and ε underlines that ε is a good indicator for the octahedral distortion Δ(O2-O2 bond length). (Lines are guide to the eyes.)

peratures, see Table I. Qualitatively, the observed structural anomalies at the antiferromagnetic ordering also agree with a mechanism based on spin-orbit coupling[42], since the elongation of the octahedron occurs parallel to the ordered spin moment pointing along the a direction, but the observed effect appears to be too large.

As can be seen in Fig. 3, we have studied a second sample of $Nd_{1-x}TiO_{3+\delta}$, which due to minor inhomogeneity exhibits a lower Néel transition at T_N=81 K. Clearly, the structural anomalies are strongly suppressed in this material.

In $LaTiO_3$ no structural anomaly is seen along the c direction, see also Ref.[35], but $NdTiO_3$ and $SmTiO_3$ exhibit such anomalies at the Néel ordering. Upon passing into the antiferromagnetic state the lattice expands along the c direction. The relative strength of these anomalies is, however, still much lower than those appearing in the ab planes. Since the ground-state orbital[5,23] in $LaTiO_3$ has significant extension along c this elongation agrees still with the orbital-ordering effect.

C. Temperature dependence of the crystal structure in Ferri-/Ferromagnetic RETiO$_3$ (RE = Gd, Y)

The temperature dependences of the lattice constants a and b in $GdTiO_3$ and in $YTiO_3$ are totally different from that in the titanates with antiferromagnetic ordering discussed above. The ferromagnetic compounds show a negative thermal-expansion coefficient along the b direction and a larger positive one along a. Again, there are well-defined anomalies around the magnetic ordering, which, however, exhibit the opposite signs compared to the antiferromagnetic compounds. The anomalies are visible in Fig. 3. In the case of $YTiO_3$ these low-temperature structural anomalies were already reported in reference[45]. The anomalies are, however, much stronger for $GdTiO_3$.

The crystal structure of $YTiO_3$ was studied by neutron diffraction on a powder sample at 35 K, i.e. slightly above T_C, and at 2 K and by single-crystal X-ray diffraction on a different sample between 100 K and room temperature. Besides the changes in the lattice constants discussed above, no significant structural changes could be detected between 100 K and room temperature. Furthermore, the powder data at 35 and 2 K did not reveal a measurable change in the crystal structure as well. The Ti-O2 bond-length distortion is rather large in $YTiO_3$, $\Delta(M-O2)$=2.91% (at 100 K), whereas the other parameter is small, $\Delta(O2-O2)$=1.08% (at 100 K). Again, the rotation and the tilt angles vary very little between room temperature and 2 K. The structural anomalies observed in these ferromagnetic titanates cannot be explained by the spin-orbit coupling. The most prominent octahedron elongation occurs along the b direction, whereas one would expect the spin-orbit coupling to cause an elongation along the c direction which is the direction of the ferromagnetic ordered moment[42]. Note, however, that indeed there is such an elongation along the c direction upon passing in the ferromagnetic state. In addition to the spin-orbit coupling, the orbital-ordering effect may also contribute to the c-axis expansion, as the lowest orbital level in $YTiO_3$ also possesses significant extension along c[18,19,23].

D. Magnetostriction and thermal-expansion measurements

In order to better resolve the structural anomalies, we have measured the thermal-expansion coefficients $\alpha = 1/L \cdot \partial L/\partial T$ for three RETiO$_3$ compounds with RE = Nd, Sm and Y (see Fig. 5) on a high-resolution capacitance dilatometer[39]. The results are given in Fig. 5 and should be compared to the similar measurement on $LaTiO_3$ described in reference[35]. For these studies we have used almost fully untwinned single crystals, as it can be ascertained by the comparison between the dilatometer and the diffraction results.

As expected from the diffraction results, the thermal-expansion anomalies in $SmTiO_3$ and in $NdTiO_3$ are much stronger than those in $LaTiO_3$; in particular the anomaly in the c parameter of $NdTiO_3$ is well resolved, whereas it has no counterpart in the high-resolution studies on $LaTiO_3$[35]. The high-resolution studies in $SmTiO_3$ and in $NdTiO_3$ confirm our conclusion that the structural anomalies set in far above the Néel ordering[43]. Furthermore, the smaller anomalies at the ferromagnetic ordering in $YTiO_3$ are confirmed by the dilatometer study. In $YTiO_3$, the c-axis anomaly is larger and the anomaly along the a direction is reversed in comparison to the antiferromagnetic compounds.

In Fig. 6 we show the results of magnetostriction experiments on $YTiO_3$. The measurement was performed approximately along the a-direction[44]. The anomaly in the thermal-expansion coefficient broadens and shifts to higher temperature with increasing magnetic field. This field dependence is expected for a ferromagnetic transition. Applying the magnetic field at low temperature well in the ferromagnetic phase, we first observe an elongation along the a direction of about $\frac{\Delta a}{a} \sim 1 \cdot 10^{-5}$. At zero field the magnetic moments in $YTiO_3$ order ferromagnetically along the c axis; under an external field along the a direction they first flip parallel to the field. The small elongation at small field can hence be associated with the reorientation of the ordered moment. This elongation is most likely caused by the spin-orbit coupling elongating the octahedron along the ordered moment[42]. This low-field magnetostriction is, however, smaller than the magnetostriction occurring at higher field. The high-field effects have to be considered as an enhancement of the integrated zero-field thermal-expansion anomalies, as it can be seen in Fig. 6 a). At zero field the ferromagnetic ordering in $YTiO_3$ is accompanied by a small antiferromagnetic moment along the a axis due to the competing magnetic interactions[46], which are determined through the orbital arrangement. Upon cooling in zero field, the orbital arrangement is changing in the way that ferromagnetism is further stabilized; this effect seems to be further strengthened by the external field which anyway stabilizes ferromagnetic order.

E. Crystal structure across the RETiO$_3$ series

Fig. 7 shows the magnetic phase diagram of RETiO$_3$ as a function of the rare-earth ionic radius. In addition to the pure RETiO$_3$ samples we have included results on samples where the A site is occupied by a mixture of La and Y. The diagram clearly shows how the crossover from ferromagnetic to antiferromagnetic order is driven by the rare-earth ionic radius, even though some influence of additional effects is visible. In the ferromagnetic RETiO$_3$, there is a stronger variation of the Curie temperature which indicates the direct influence of the RE-Ti magnetic interaction. Non-magnetic Y implies a comparably low Curie temperature in this series. Nevertheless, the

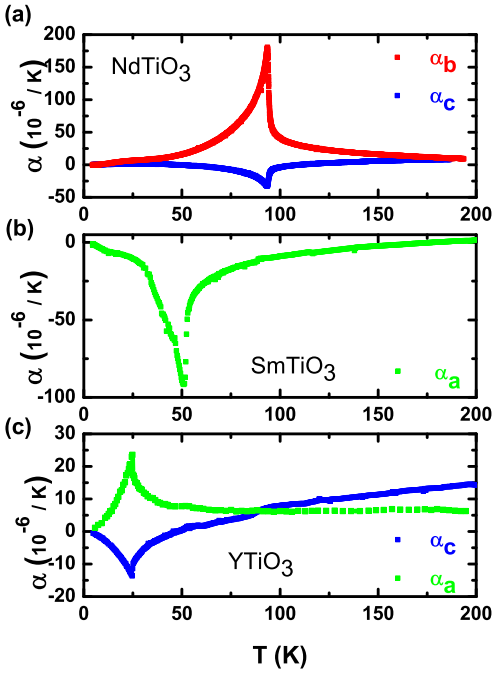

FIG. 5: (color online) Thermal expansion $\alpha = 1/l \cdot \partial l/\partial T$ for (a) $NdTiO_3$ parallel to b and c, (b) $SmTiO_3$ parallel to a and (c) $YTiO_3$ parallel to a and c.

rare-earth ionic radius can be considered as the main external parameter driving the magnetic transition in the pure as well as in the mixed compounds.

In Fig. 8 the results of our single crystal diffraction measurements performed at room temperature are resumed. Qualitatively, these results agree with previous studies[4] but there are significant quantitative differences due to the improved sample quality and due to he higher precision rendered possible with the modern CCD-X-ray techniques.

Both $NdTiO_3$ crystals with T_N of 94 K and of 81 K were studied at room temperature. The lower T_N of the second crystal already indicates some non-stoichiometry. With X-ray diffraction it is difficult to determine precisely the oxygen content, therefore, it is not astonishing that the change in the refined oxygen content per formula unit from 2.952(30) (high-T_N sample) to 2.988(12) (low-T_N sample) is not very significant. However, in the low-T_N sample we find a significant amount of vaccancies on the Nd-site with a content per formula unit of only 0.979(1), whereas the high-T_N sample as well as the other RETiO$_3$ compounds with high transition temperatures show the ideal RE to Ti ratio within comparable precision. The structural parameters obtained for the low-T_N and high-T_N samples are comparable in view of the large variation of the internal parameters in the RETiO$_3$ series, see Table I, however clear differences can be detected. The main influence of the excess oxygens consists in a reduction of the octahedron tilting. Since excess oxygen and Nd-vacancies enhance the Ti valence

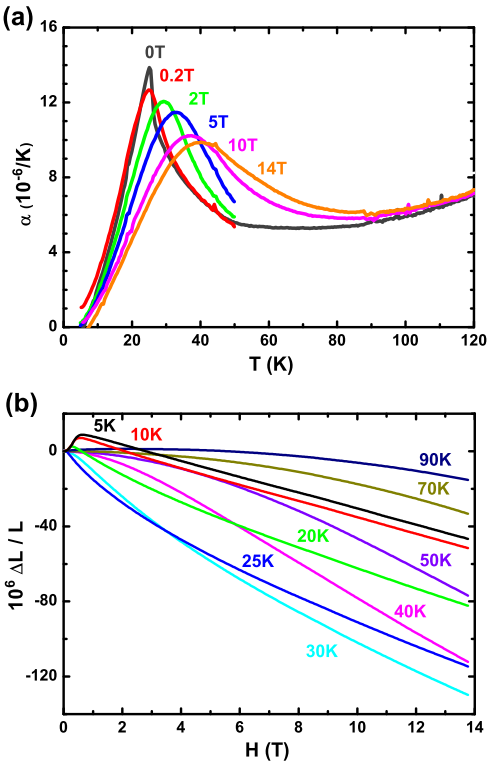

FIG. 6: (color online) (a) Thermal expansion $\alpha = 1/l \cdot \partial l/\partial T$ of $YTiO_3$ for various magnetic fields as a function of temperature ($H \| a$). (b) Magnetostriction $\Delta L(H)/L$ of $YTiO_3$ as a function of applied magnetic field $H \| a$.

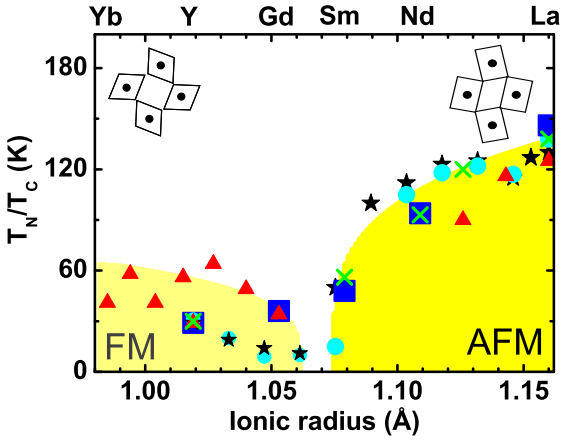

FIG. 7: (color online) Magnetic phase diagram for RETiO$_3$ and La$_{1-x}$Y$_x$TiO$_3$. T$_C$ and T$_N$ are plotted as a function of the rare-earth ionic radius. Squares: T$_C$/T$_N$ for RETiO$_3$ from this work, triangles: values for RETiO$_3$ from Greedan[29], crosses: values for RETiO$_3$ from Katsufuji *et al.*[51], circles: values for La$_{1-x}$Y$_x$TiO$_3$ from Okimoto *et al.*[3], stars: values for La$_{1-x}$Y$_x$TiO$_3$ from Goral *et al.*[52]. The inserts show the principal octahedral deformations of the end members.

and thereby reduce the effective Ti-ionic radius, this tilt reduction is in perfect agreement with the bond-length mismatch scenario described by the tolerance factor. A similar suppression of the tilt distortion by excess oxygen was also found in La$_2$CuO$_{4+\delta}$[47]. The enhanced Ti-valency in the non-stoichiometric sample is directly observed in the bond-valence sum which is 0.045(1) larger than that in the stoichiometric compound.

In Fig. 8 we plot the structural parameters against the rare-earth ionic radius. The largest overall structural changes concern the tilt and the rotation deformations. The decrease of the rare-earth ionic radius enhances the bond-length mismatch and these angles, as seen in Fig. 8 (a) and in the Ti-O-Ti angles shown in Fig. 8 (b). The distortion of the ideal perovskite structure gets extremely strong for $YTiO_3$ which appears close to the stability of the *Pbnm* structure. Due to increasing tilt and rotation deformations the RE-O distances vary strongly within the series; the ratio of the longest to the shortest bond increases from 1.42 in $LaTiO_3$ to 1.63 in $YTiO_3$. For a rigid tilt an O1 site directly moves towards a RE site yielding the shortest RE-O bond in the entire series (RE-O distance #6 in Fig. 8). This short bond seems to cause the inversed orthorhombic splitting seen in many weakly distorted perovskites, as discussed above. For the smaller rare earths, however, the systems seems to avoid the extremely short RE-O1 bond distance by shifting the RE site. As can be seen in Fig. 8 (g) the shift of the RE site with respect to its high-symmetry position at (0.5,0,0.25) varies stronger than the oxygen internal parameters related with the tilting. Due to this RE shift, the shortest RE-O1 distance does not get very small and at the same time the distance to the opposed O1 sites increases less, see Fig. 8 (c). Furthermore, the RE-site shift in y direction results in a strong splitting of the two distances to the two O1 sites near (0.5,±0.5,0.25). The structural change implied through the smaller ionic radius in the RETiO$_3$ series is, therefore, not only described by the increasing tilt and rotation angles, but in addition there is a change in the RE-O coordination.

With the increasing shift of the RE site for smaller rare-earth ionic radius the deformation of the RE-Ti coordination increases as well, as it is shown in Fig. 8 (h). In the cubic perovskite, each RE has eight nearest Ti neighbors; these distances significantly split for the smaller RETiO$_3$ most likely destabilizing the orbital arrangement of the $LaTiO_3$ type[5,23].

For the Ti-orbital physics the internal parameters of the TiO_6 octahedra are important. In agreement with the previous discussion[5] there is a crossover in the octahedral distortion through the RETiO$_3$ series. Whereas $LaTiO_3$ exhibits the rectangular elongation of the basal plane characterized by $\Delta(O2 - O2)$, $YTiO_3$ exhibits the rhombic distortion characterized through distinct in-plane Ti-O bond distances and $\Delta(M - O2)$. As stressed in reference[5], this structural crossover is accompanied by the magnetic crossover from the antiferromagnetic to the ferromagnetic ground state. A part of this crossover seems to be induced by the structural effects discussed

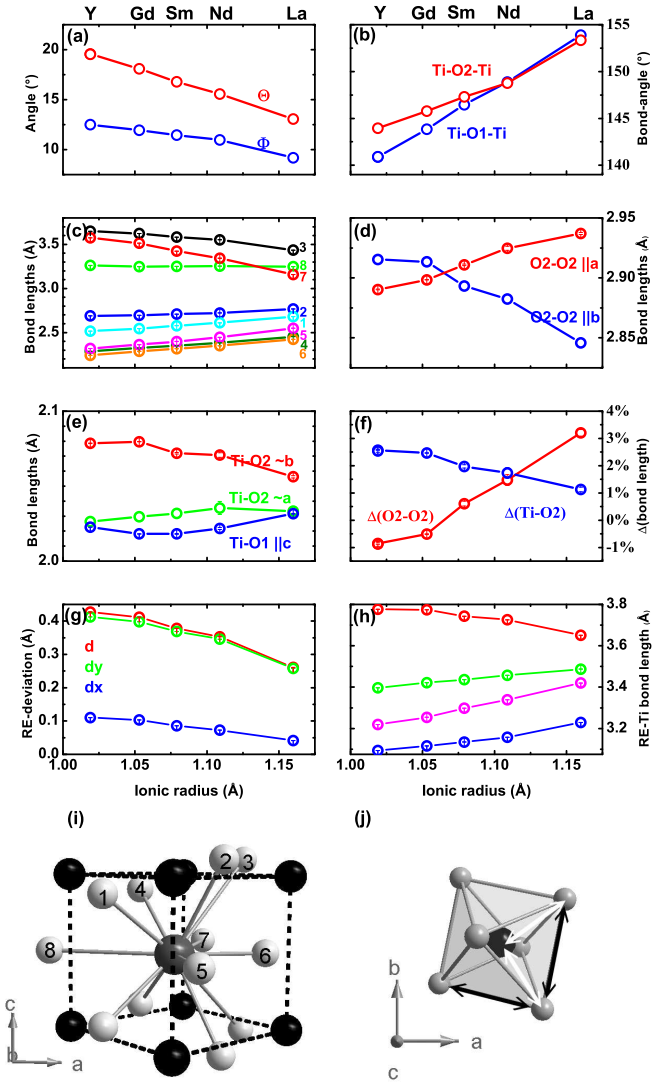

FIG. 8: (color online) Results from single crystal X-ray diffraction measurements at room temperature (open circles). (a) Apical tilt Θ and basal rotation Φ of the TiO_6 octahedra of RETiO$_3$. (b) Ti-O-Ti bond angles. (c) RE-O bond lengths (see plot (g) for notation). (d) O2-O2 bond lengths. (e) Ti-O bond lengths. (f) ratio of O2-O2 bond lengths and ratio of Ti-O2 bond lengths (see also plot (h)). (g) Displacement of the RE ion from the symmetry position $00\frac{1}{4}$. (h) RE-Ti bond lengths. (i) Oxygen coordination of the RE^{3+} ion with the numbering for plot (c). (j) TiO_6 - black arrows indicate both O2-O2 bonds which are about parallel to a or b and white arrows indicate the two Ti-O2 bonds which are rotated by Φ towards a or $-b$.

above, i.e. the response of the RE-O arrangement to the extremely strong tilt and rotation distortions. For the smaller rare earths the displacement of the RE site is more important and has a stronger direct influence on the crystal-field splitting of the t_{2g} levels. This purely structural explanation of part of the deformation is further supported by the similar effects occurring in the REFeO$_3$ series, whose structure was studied in detail[48,49,50]. The REFeO$_3$ series shows almost the identical tilt and rotation angles as a function of rare-earth ionic radius causing similar constraints in the RE-O coordination. Interestingly also this system exhibits the octahedral basal-plane elongation for larger rare earths and the Fe-O2 bond distance splitting for smaller rare earths, but both effects are much weaker than in the case of the corresponding titanates.

With the analysis of the intrinsic structural response to the smaller rare-earth ionic radius we may more deeply discuss the structural anomalies occurring in all RETiO$_3$ studied as a function of temperature. It appears that the tilt, the rotation and the RE-site shifts implied through the rare-earth ionic radius already favor a certain crystal-field splitting[22,23], which in case of LaTiO$_3$ results in a ferroorbital ordering (within the ab-plane) whereas it causes an antiferroorbital ordering in YTiO$_3$. The compounds close to the structural crossover, where the nature of the lowest orbital level should change as well, appear most interesting. The ferroorbital and the antiferroorbital ordering imply an antiferromagnetic and a ferromagnetic nearest-neighbor magnetic interaction, respectively. Close to the structural and magnetic crossover the magnetic interaction is hence significantly reduced in agreement with the lower values of T_C and T_N (see Fig. 7). Upon cooling, each of the titanates passes into a well ordered state and in order to suppress the magnetic fluctuations the magnetic interaction parameters should get enhanced on the cost of a lattice deformation. Since either the ferromagnetic or the antiferromagnetic interaction should increase upon cooling, either the antiferroorbital (RE= Gd, Y) or the ferroorbital (RE=La, Nd, Sm) ordering (within the ab-plane) must get enhanced by rotating the orbital degree of freedom. This explains first the sign change of the in-plane anomalies in the series and second the observation of the strongest anomalies in the compounds close to the crossover. Upon continuously varying the magnetic nearest-neighbor interaction J, it has to pass zero which due to the diverging magnetic fluctuations yields an energetically unfavorable phase. In all compounds, the orbital effects follow the crystal-field splitting implied by the structural deformation, thereby enhancing the magnetic interaction.

As suggested in the phase diagram shown in Fig. 7 the rare-earth ionic radius should be considered as the external parameter driving the magnetic transition from antiferromagnetic to ferromagnetic ordering. Therefore, the RETiO$_3$ phase diagram may be compared to the many known systems where a magnetic transition may be implied by varying some external control parameter. As it has been recently discussed for a generic quantum phase transition one may expect a sign change in the thermal-expansion anomalies when crossing the transition[53] due to the fact that the system will avoid the accumulation of entropy just at the transition. The sign changes in the thermal-expansion anomalies were for example observed across the metamagnetic transition in $Ca_{2-x}Sr_xRuO_4$[54].

F. $La_{1-x}Y_xTiO_3$ (x=0.50)

Since the rare-earth ionic radius drives the structural deformations, the orbital arrangement and the magnetic structure, it would be quite interesting to study this phase diagram by continuously varying the ionic radius. $La_{1-x}Y_xTiO_3$ was thought to be a good system since there is no magnetic moment on the *RE* site. Several groups have already studied this system, see references[51,52]. Indeed this system shows the transition from antiferromagnetism to ferromagnetism between 30 and 40 % of Y[52]. We have prepared a powder sample of $La_{0.50}Y_{0.50}TiO_3$ and show the inverse of its magnetic susceptibility in Fig. 9 (*b*). There is no well-defined anomaly comparable to the effects in the pure $RETiO_3$ but the weak effect around 90 K indicates the onset of antiferromagnetic ordering in qualitativ agreement with the Curie-Weiss analysis of the susceptibility at higher temperatures. From these magnetic properties and from the averaged ionic radius which is between those of Nd and Sm one would expect similar physical properties as those observed in $NdTiO_3$ and in $SmTiO_3$. Fig. 9 (*a*) shows, however, that this is not the case. Although the orthorhombic lattice parameters are in between the corresponding values of the pure Nd and Sm compounds, comparable structural anomalies at low temperatures do not occur in $La_{0.50}Y_{0.50}TiO_3$, see the plot of the orthorhombic distortion in Fig. 9 (*a*). We think that the disorder arising from the mixed occupation of La and Y with quite different ionic radii destroys the effects induced by orbital ordering. Although this result annihilates the hope to tune a mixed titanate to the critical averaged rare-earth ionic radius and to drive it thereby into a critical configuration, it corroborates our conclusion that the structural anomalies in the $RETiO_3$ materials arise from orbital physics.

IV. CONCLUSION.

The detailed structural analysis of the $RETiO_3$ series as a function of temperature allows us to separate the structural effects implied directly through the variation of the rare-earth ionic radius from those related with an orbital effect. The decrease of the rare-earth ionic radius leads first to the enhancement of the tilt and rotation angles and second to a modification of the *RE*-O and *RE*-Ti coordinations. For small distortion angles the *RE*-site is closer to its high-symmetry position whereas it moves away from that for the larger distortions. As has been stated by several groups these shifts yield already a significant crystal field splitting of the t_{2g} levels. The character of the thereby lowered orbital is rather different and the orbital arrangement, which is either ferroorbital or antiferroorbital in nature, is even opposed for the end-members of the series.

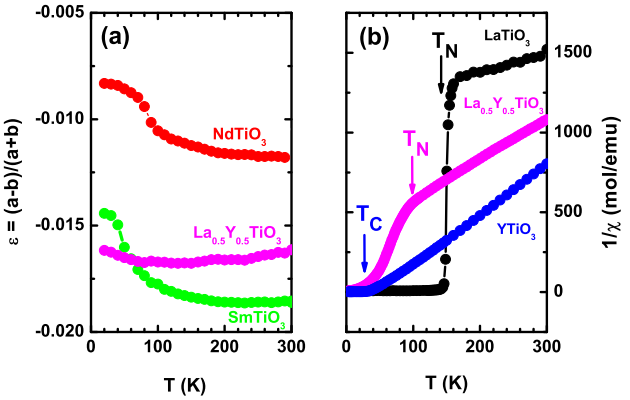

FIG. 9: (color online) (a) Orthorhombic splitting ε of $La_{1-x}Y_xTiO_3$ (x=0.50) compared with the other $RETiO_3$ with similar rare earth ionic radii. (b) Inverse magnetic susceptibility $1/\chi$ of $La_{0.5}Y_{0.5}TiO_3$ compared with $LaTiO_3$, $YTiO_3$ and the average of $LaTiO_3$ and $YTiO_3$. Arrows indicate T_C/T_N.

The temperature dependence of the crystal structure, however, shows that anomalous structural deformations occur in all $RETiO_3$ which should modify the character of the orbital with the lowest energy. Since the ferroorbital and antiferroorbital *ab*-plane arrangement is related with an antiferromagnetic and ferromagnetic nearest-neighbor interaction, respectively, the structural change directly couples to the magnetism. The structural anomalies are clearly associated with the magnetic ordering temperatures where the thermal-expansion coefficients exhibit extrema. We, therefore, conclude that magnetism drives a change in the orbital ground state. In all compounds, this change points in the sense to enhances the dominant magnetic interaction. For antiferromagnetic $RETiO_3$ with La, Nd and Sm the ferroorbital arrangement is strengthened while for $GdTiO_3$ and $YTiO_3$ the antiferroorbital arrangement is strengthened. In this sense the temperature-driven orbital ordering follows the crystal-field splitting already imposed through the strong distortions. The structural effects are weakest in the end members and strongest close to the structural and magnetic crossover. Unfortunately, it seems not possible to drive the titanates into the critical configuration by continuously varying the ionic radius in a mixed system $La_{1-x}Y_xTiO_3$ as disorder effects seem to suppress orbital degrees of freedom.

V. ACKNOWLEDGEMETS.

This work was supported by the Deutsche Forschungsgemeinschaft through Sonderforschungsbereich 608. We

RE:	***La***‡	***Nd***†	***Nd****†	***Sm***	***Sm***	***Sm***	***Gd***	***Y***	***Y***
T (K)	***290***	***290***	***290***	***290***	***130***	***100***	***290***	***290***	***200***
Data:									
obs. refl.	21502	24349	16509	34784	4265	4830	18460	23944	4779
av. refl.	1557	1516	1076	4507	1814	2202	4139	2925	721
redund.	13.81	16.06	15.34	7.72	2.35	2.19	4.46	8.19	6.63
$\mathbf{R}_{int}$	2.68%	3.23%	2.45%	2.83%	2.26%	2.13%	2.41%	2.85%	2.84%
$\mathbf{2\Theta}_{max}$	76°	107.7°	68.8°	132.3°	84.1°	95.1°	134.3°	112.6°	79.1°
Lattice:									
a (Å)	5.63676(25)	5.52532(87)	5.51917(15)	5.4647(2)	5.4643(2)	5.4651(2)	5.4031(2)	5.3425(2)	5.3210(7)
b (Å)	5.61871(26)	5.65945(88)	5.63593(16)	5.6712(2)	5.6669(2)	5.6626(2)	5.7009(2)	5.6925(2)	5.6727(7)
c (Å)	7.91615(34)	7.79066(121)	7.79506(22)	7.7291(3)	7.7154(3)	7.7133(3)	7.6739(2)	7.6235(2)	7.5949(10)
Atoms:									
x(RE1)	0.99265(1)	0.98691(2)	0.98788(1)	0.98441(1)	0.98471(3)	0.98473(2)	0.98092(1)	0.97937(2)	0.97873(4)
y(RE1)	0.04587(3)	0.06103(2)	0.05788(1)	0.06501(1)	0.06476(3)	0.06488(3)	0.06985(1)	0.072475(2)	0.07324(4)
z(RE1)	0.25	0.25	0.25	0.25	0.25	0.25	0.25	0.25	0.25
x(Ti1)	0	0	0	0	0	0	0	0	0
y(Ti1)	0.5	0.5	0.5	0.5	0.5	0.5	0.5	0.5	0.5
z(Ti1)	0	0	0	0	0	0	0	0	0
x(O1)	0.0809(2)	0.0962(3)	0.0932(1)	0.1026(1)	0.1008(5)	0.1010(4)	0.1102(2)	0.1188(1)	0.1195(3)
y(O1)	0.49079(18)	0.4792(4)	0.4787(3)	0.4725(2)	0.4743(4)	0.4742(4)	0.4662(2)	0.4587(1)	0.4587(3)
z(O1)	0.25	0.25	0.25	0.25	0.25	0.25	0.25	0.25	0.25
x(O2)	0.70975(11)	0.7005(2)	0.7013(1)	0.6975(1)	0.6975(3)	0.6976(3)	0.6943(1)	0.6909(1)	0.6908(2)
y(O2)	0.29348(13)	0.3019(2)	0.3006(1)	0.3039(1)	0.3035(3)	0.3037(3)	0.3064(1)	0.3085(1)	0.3090(2)
z(O2)	0.04210(9)	0.0487(2)	0.0472(1)	0.0515(1)	0.0514(2)	0.0516(2)	0.0541(1)	0.0576(1)	0.0577(2)
U_{ij} *(Å^2):*									
$\mathbf{U}_{11}$**(RE1)**	0.00463(6)	0.00740(4)	0.00633(4)	0.00500(2)	0.0053(1)	0.00497(6)	0.00732(2)	0.00517(4)	0.0041(1)
$\mathbf{U}_{22}$**(RE1)**	0.00470(6)	0.00671(5)	0.00608(5)	0.00427(2)	0.0038(1)	0.00364(6)	0.00626(2)	0.00391(4)	0.0036(1)
$\mathbf{U}_{33}$**(RE1)**	0.00456(5)	0.00674(5)	0.00528(5)	0.00445(2)	0.0048(1)	0.00452(7)	0.00731(2)	0.00523(4)	0.0041(1)
$\mathbf{U}_{12}$**(RE1)**	-0.00077(2)	-0.00069(3)	-0.00087(3)	-0.00071(1)	-0.00059(4)	-0.00055(3)	-0.00046(1)	-0.00041(3)	-0.0003(1)
$\mathbf{U}_{13}$**(RE1)**	0	0	0	0	0	0	0	0	0
$\mathbf{U}_{23}$**(RE1)**	0	0	0	0	0	0	0	0	0
$\mathbf{U}_{11}$**(Ti1)**	0.00226(18)	0.00541(9)	0.0034(1)	0.00308(4)	0.0035(2)	0.0036(1)	0.00576(6)	0.00375(7)	0.0027(2)
$\mathbf{U}_{22}$**(Ti1)**	0.00258(19)	0.00517(11)	0.0021(1)	0.00311(4)	0.0030(2)	0.0029(2)	0.00561(6)	0.00398(7)	0.0033(2)
$\mathbf{U}_{33}$**(Ti1)**	0.00249(15)	0.00500(12)	0.0031(1)	0.00241(4)	0.0032(2)	0.0030(2)	0.00553(6)	0.00325(7)	0.0019(2)
$\mathbf{U}_{12}$**(Ti1)**	-0.00005(6)	-0.00006(9)	-0.00005(9)	0.00000(3)	-0.00002(13)	-0.00007(10)	-0.00005(4)	-0.00014(5)	-0.0002(1)
$\mathbf{U}_{13}$**(Ti1)**	-0.00005(5)	0.00001(7)	-0.00012(6)	-0.00005(3)	-0.00004(12)	-0.00008(10)	-0.00004(4)	-0.00025(5)	-0.0003(1)
$\mathbf{U}_{23}$**(Ti1)**	-0.00020(8)	-0.00002(10)	-0.00033(9)	0.00002(3)	-0.00001(15)	-0.00004(11)	0.00012(4)	0.00006(5)	-0.0000(1)
$\mathbf{U}_{11}$**(O1)**	0.0073(5)	0.00951(46)	0.0089(4)	0.0070(2)	0.0081(9)	0.0080(7)	0.0092(3)	0.0084(3)	0.0052(7)
$\mathbf{U}_{22}$**(O1)**	0.0097(5)	0.00904(58)	0.0104(6)	0.0072(2)	0.0051(9)	0.0043(7)	0.0087(3)	0.0070(3)	0.0050(7)
$\mathbf{U}_{33}$**(O1)**	0.0055(4)	0.00500(59)	0.0061(6)	0.0034(2)	0.0049(9)	0.0046(7)	0.0064(3)	0.0059(3)	0.0022(8)
$\mathbf{U}_{12}$**(O1)**	-0.0002(3)	-0.00128(45)	0.0026(3)	-0.0013(2)	-0.0017(7)	-0.0014(5)	-0.0013(2)	-0.0015(2)	-0.0010(5)
$\mathbf{U}_{13}$**(O1)**	0	0	0	0	0	0	0	0	0
$\mathbf{U}_{23}$**(O1)**	0	0	0	0	0	0	0	0	0
$\mathbf{U}_{11}$**(O2)**	0.0064(3)	0.0082(3)	0.0069(2)	0.0056(1)	0.0065(6)	0.0057(5)	0.0082(2)	0.0076(2)	0.0045(5)
$\mathbf{U}_{22}$**(O2)**	0.0072(3)	0.0075(4)	0.0037(4)	0.0053(2)	0.0041(6)	0.0041(5)	0.0076(2)	0.0069(2)	0.0042(5)
$\mathbf{U}_{33}$**(O2)**	0.0087(3)	0.0090(5)	0.0090(4)	0.0070(2)	0.0066(6)	0.0069(6)	0.0095(2)	0.0091(3)	0.0055(6)
$\mathbf{U}_{12}$**(O2)**	-0.0018(2)	-0.0018(3)	-0.0012(2)	-0.0016(1)	-0.0015(5)	-0.0009(4)	-0.0014(2)	-0.0016(2)	-0.0002(1)
$\mathbf{U}_{13}$**(O2)**	0.0008(2)	0.0007(3)	0.0014(2)	0.0009(1)	0.0005(4)	0.0007(3)	0.0009(2)	0.0014(2)	0.0009(4)
$\mathbf{U}_{23}$**(O2)**	-0.0074(2)	-0.0009(4)	-0.0016(3)	-0.0014(1)	-0.0011(5)	-0.0010(4)	-0.0014(2)	-0.0017(2)	-0.0011(4)
Fit:									
GoF	2.29	2.40	1.22	2.09	2.54	2.56	2.33	2.11	2.07
R	1.32%	2.11%	1.62%	1.34%	1.95%	1.99%	1.82%	1.70%	1.89%
$\mathbf{R}_w$	2.97%	3.87%	4.30%	2.46%	4.77%	4.96%	3.53%	2.53%	3.92%

TABLE I: Results of single crystal X-ray diffraction measurements of RETiO$_3$ (RE = La, Nd, Sm, Gd, Y) at room temperature and for RE = Sm, Y down to 100 K. *: results for a (non-stoichiometric) NdTiO$_3$-sample with T$_N$ = 81 K. ‡: The LaTiO$_3$ single crystal was twinned with the following ratios of the six possible domains: 82.7%, 8.1%, 4.2%, 1.8%, 1.5% and 1.5%. †: Both NdTiO$_3$-crystals were slightly twinned ($a \leftrightarrow b$) with a major twin domain of roughly 90% and all reflections with $|h-k| \leq 1$ ($h, k \neq 0$) were excluded as they could not be separated from other twin contributions in the integration procedure.

thank D. Khomskii for valuable discussions, N. Schittner and N. Hollmann for various susceptibility measurements and D. Meier, J. Rohrkamp and O. Heyer for some thermal expansion experiments.

* Electronic address: braden@ph2.uni-koeln.de

[1] M. Imada, A. Fujimori, and Y. Tokura, Rev. Mod. Phys. **70**, 1039 (1998).
[2] R. D. Shannon, Acta Crystallographica **A32**, 751 (1976).

RE:	***La***	***La***	***Y***	***Y***
T (K)	***550***	***747***	***2***	***35***
$\mathbf{M}_c$ (μ_B/**Ti^{3+}**)	0	0	0.753(75)	0
lattice:				
a (Å)	5.6386(2)	5.6454(2)	5.3226(1)	5.3239(1)
b (Å)	5.6367(2)	5.6447(2)	5.6952(1)	5.6944(1)
c (Å)	7.9518(2)	7.9699(3)	7.5962(2)	7.5952(2)
atoms:				
x(RE1)	0.9928(5)	0.99329(1)	0.9776(2)	0.9780(2)
y(RE1)	0.0387(2)	0.0353(3))	0.0740(1)	0.0738(2)
z(RE1)	0.25	0.25	0.25	0.25
x(Ti1)	0	0	0	0
y(Ti1)	0.5	0.5	0.5	0.5
z(Ti1)	0	0	0	0
x(O1)	0.0778(5)	0.0759(7)	0.1213(2)	0.1212(2)
y(O1)	0.4882(4)	0.4885(5)	0.4570(2)	0.4572(2)
z(O1)	0.25	0.25	0.25	0.25
x(O2)	0.7102(4)	0.7113(5)	0.6901(1)	0.6901(2)
y(O2)	0.2908(4)	0.2896(5)	0.3092(2)	0.3095(2)
z(O2)	0.0401(2)	0.0391(3)	0.0577(1)	0.0576(1)
B (Å^2):				
B(RE1)	1.07(2)	1.33(3)	0.177(12)	0.193(12)
B(Ti1)	0.55(3)	0.70(4)	0.190(25)	0.181(26)
B(O1)	1.05(3)	1.32(4)	0.257(16)	0.305(17)
B(O2)	1.21(3)	1.60(3)	0.228(10)	0.264(10)
fit:				
R	4.31%	4.45%	3.61%	3.70%
$\mathbf{R}_w$	5.78%	5.93%	4.89%	4.91%

TABLE II: Results of the rietveld refinement of powder neutron diffraction measurements of RETiO$_3$ (RE = La and Y) at different temperatures.

[3] Y. Okimoto, T. Katsufuji, Y. Okada, T. Arima und Y. Tokura, Phys. Rev. B **51**, 9581 (1995).

[4] D. A. MacLean, H.-N. Ng und J. E. Greedan, J. Solid State Chem. **30**, 35 (1979).

[5] M. Cwik, T. Lorenz, J. Baier, R. Müller, G. Andre, F. Bouree, F. Lichtenberg, A. Freimuth, E. Müller-Hartmann und M. Braden, Phys. Rev. B **68**, 060401 (2003).

[6] G. Amow and J. E. Greedan, Journal of Solid State Chemistry **121**, 443-450 (1996).

[7] G. Amow, J. E. Greedan and C. Ritter, Journal of Solid State Chemistry **141**, 262-269 (1996).

[8] B. Keimer, D. Casa, A. Ivanov, J. W. Lynn, M. v. Zimmermann, J. P. Hill, D. Gibbs, Y. Taguchi and Y. Tokura, Phys. Rev. Letters **85**, 3946 (2000).

[9] G. I. Meijer, W. Henggeler, J. Brown, O.-S. Becker, J. G. Bednorz, C. Rossel and P. Wachter, Phys. Rev. B **59**, 11832 (1999).

[10] C. C. Hays, J. S. Zhou, J. T. Markert and J. B. Goodenough, Phys. Rev. B **60**, 10367 (1999).

[11] J. P. Goral and J. E. Greedan, J. Magn. Matter **37**, 315 (1983).

[12] J. Akimitsu, H. Ichikawa, N. Eguchi, T. Miyano, M. Nishi and K. Kakurai, J. Phys. Soc. Japan **70**, 3475 (2001).

[13] J. D. Garrett and J. E. G. D. A. MacLean, Mater. Res. Bull. **16**, 145 (1981).

[14] M. Onoda and M. Yasumoto, J. Phys.: Condens. Matter **9**, 3861 (1997).

[15] M. Onoda and M. Yasumoto, J. Phys.: Condens. Matter **9**, 5623 (1997).

[16] H. D. Zhou and J. B. Goodenough, J. Phys.: Condens. Matter **17**, 7395 (2005).

[17] E. F. Bertaut, Acta. Cryst. A **24**, 217 (1968)

[18] I. Solovyev, Phys. Rev. B **69**, 134403 (2004)

[19] I. Solovyev, Phys. Rev. Lett. **74**, 054412 (2006)

[20] G.Khaliullin and S. Maekawa, Phys. Rev. Lett. **85**, 3950 (2000).

[21] G. Khaliullin, Phys. Rev. B **64**, 212405 (2001).

[22] M. Moshizuki and M. Imada, J. Phys. Soc. Jpn. **70**, 2872 (2001).

[23] E. Pavarini, S. Biermann, A. Poteryaev, A. I. Lichtenstein, A. Georges and O.K. Andersen, Phys. Rev. Lett. **92**, 176403 (2004).

[24] R. Schmitz, O. Entin-Wohlman, A. Aharony, A. B. Harris, and E. Müller-Hartmann Phys. Rev. B **71**, 214438 (2005)

[25] R. Schmitz, O. Entin-Wohlman, A. Aharony, A. B. Harris, and E. Müller-Hartmann Phys. Rev. B **71**, 144412 (2005)

[26] M. W. Haverkort et al. Phys. Rev. Lett. **94**, 056401 (2005).

[27] R. Rückamp, E. Benckiser, M. W. Haverkort, H. Roth, T. Lorenz, A. Freimuth, L. Jongen, A. Möller, G. Meyer, P. Reutler, B. Büchner, A. Revcolevschi, S.-W. Cheong, C. Sekar, G. Krabbes and M. Grüninger, New J. Phys. **7**, 144 (2005).

[28] C. W. Turner, M. F. Collins and J. E. Greedan, J. Magn. Magn. Mater. **23**, 265 (1981).

[29] J. E. Greedan, J. Less Common Metals **111**, 335 (1985).

[30] M. Heinrich, H.-A. Krug von Nidda, V. Fritsch, and A. Loidl, Phys. Rev. B **63**, 193103 (2001).

[31] C. W. Turner and J. E. Greedan, J. Solid State Chem. **34**, 207 (1980).

[32] D. I. Khomskii and G. Sawatzky, Sol. State Commun. **102**, 87 (1997).

[33] J. Rodriguez-Carvajal, F. Moussa, M. Hennion, H. Moudden, L. Pinsard and A. Revcolevschi, Phys. Rev. B **57**, 3189 (1998).

[34] T. Mizokawa und A. Fujimori, Phys. Rev. B **54**, 5368 (1996).

[35] J. Hemberger, H.-A. Krug von Nidda, V. Fritsch, J. Deisenhofer, S. Lobina, T. Rudolf, P. Lunkenheimer, F. Lichtenberg, A. Loidl, D. Bruns and B. Büchner, Phys. Rev. Lett **91**, 066403 (2003).

[36] H. Roth, unpublished.

[37] International Tables of Crystallography, Vol. A, V. edition, Kluwer academic publishers (2002).

[38] http://www-xray.fzu.cz/jana/Jana2000/jana.html

[39] T. Lorenz, U. Ammerahl, B. Büchner, and A. Revcolevschi, Phys. Rev. B **55**, 5914 (1997).

[40] Inorganic crystal structure database (ICSD) http://icsdweb.fiz-karlsruhe.de/.

[41] We excluded $TbAlO_3$ as the atomic positions were determined by powder X-ray diffraction with the consequence of larger errors.

[42] K.I. Kugel and D.I. Khomskii, Sov. Phys. Usp. **25**, 231 (1982).

[43] The overall agreement between the macroscopic thermal expansion experiment and the diffraction results indicates that these samples are nearly untwinned, with the minority domains containing about 10% of the total volume.

[44] Most likely due to an imperfect orientation, about 15% of other directions are superposed explaining the weaker anomaly at T_C when compared to the thermal expansion experiment.

[45] H. Nakao, Y. Wakabayashi, T. Kiyama, Y. Murakami, M. v. Zimmermann, J. P. Hill, Doon Gibbs, S. Ishihara, Y. Taguchi and Y. Tokura, Phys. Rev. B **66**, 184419 (2002).

[46] C. Ulrich, G. Khaliullin, S. Okamoto, M. Reehuis,

A. Ivanov, H. He, Y. Taguchi, Y. Tokura and B. Keimer, Phys. Rev. Lett. **89**, 167202 (2002).
[47] M. Braden, P.Schweiss, G. Heger, W. Reichardt, Z. Fisk, K. Gamayunov, I. Tanaka and H. Kojima, Physica C **223**, 396 (1994).
[48] M. Marezio and P. D. Dernier, Mater. Res. Bull. **6**, 23 (1971).
[49] M. Marezio, J. P. Remeika, and P. D. Dernier, Acta Crystallogr. Sect. B: Struct. Crystallogr. Cryst. Chem. **26**, 2008 (1970).
[50] J.-S. Zhou, J. B. Goodenough, and B. Dabrowski, Phys. Rev. B **70**, 081102(R) (2004)
[51] T. Katsufuji, Y. Taguchi, and Y. Tokura, Phys. Rev. B **56**, 10145 (1997).
[52] J. P. Goral, J. E. Greedan und D. A. MacLean, Journal of Solid State Chemistry **43**, 244 (1982).
[53] M. Garst and A. Rosch, Phys. Rev. B **72**, 205129 (2005).
[54] M. Kriener, P. Steffens, J. Baier, O. Schumann, T. Zabel, T. Lorenz, O. Friedt, R. Müller, A. Gukasov, P. Radaelli, P. Reutler, A. Revcolevschi, S. Nakatsuji, Y. Maeno and M. Braden, Phys. Rev. Lett. **95**, 267403 (2005).